A pH-dependent binding of chloride to a marine alkaline phosphatase affects catalysis, active site stability and dimer equilibrium

Jens. G. Hjörleifsson* and Bjarni Ásgeirsson*

Department of Biochemistry, Science Institute, University of Iceland, Dunhagi 3, 107 Reykjavik, Iceland.

Keywords: Alkaline phosphatase, ionic interactions, enzyme kinetics, dimer, metal ions, periplasmic space.

Abstract

The effect of ionic strength on enzyme activity and stability varies considerably between enzymes. Ionic strength is known to affect the catalytic activity of some alkaline phosphatases (AP), such as the *E. coli* AP, but how ions affect APs is debated. Here, we studied the effect of various ions on a cold-adapted AP from *Vibrio splendidus (*VAP). Previously, we have found that the active form of VAP is extremely unstable at low ionic strength. Here we showed that NaCl increased both activity and stability of VAP, and that the effect was pH dependent in the range of 7–10. The activity profile as a function of pH formed two maxima, indicating a possible conformational change. Bringing the pH from the neutral to the alkaline range was accompanied by a large increase in both K_i for inorganic phosphate (product inhibition) and K_M for p-nitrophenyl phosphate. The activity transitions observed as the pH was varied correlated with structural changes as monitored by tryptophan fluorescence. Thermal and urea induced inactivation was shown neither to be accompanied by dissociation of the active site metal ions nor dimer dissociation. This would suggest that the inactivation involved subtle changes in active site conformation. Furthermore, VAP dimer equilibrium was studied for the first time and shown to highly favor dimerization which was dependent on pH and NaCl concentration. Taken together, the data support a model where anions bind to some specific acceptor in the active site of VAP, resulting in great stabilization and catalytic rate enhancement, presumably through a different mechanism.

Introduction

Environmental factors, such as heat, pH and ionic strength place enzymes under evolutionary pressure to adapt by residue replacements [1-3]. For multicellular organisms, the ionic strength is maintained relatively constant both inside cells and in extracellular spaces. However, bacteria have evolved to withstand environments of various ionic strength. In sea ice, for example, microbes are found in habitats created by pores and channels in the sea ice, where salinity can vary from 0–200% [4, 5].

The effects of ions on the function and stability of enzymes have been extensively studied but vary depending on the enzyme. Different effects may be observed in low concentrations (salting-in), where effects may be due to semi-specific binding of the ions to the enzyme, or higher concentration (salting-out), where the properties of the water medium might be affected (Hofmeister effects). The intricacies of these interactions are not yet fully understood [6, 7].

The alkaline phosphatase (AP) superfamily is well-suited to studying the evolution of enzymes due to environmental factors, since it is only found as an extracellular enzyme, either secreted or membrane-bound. APs are homodimeric metalloenzymes containing two zinc ions and one magnesium ion in each active site. The Zn^{2+} ions have both a substrate binding role and a role in hydrolysis, while the Mg^{2+} ion is believed to activate the nucleophilic Ser in the active site [8]. In Gram-negative bacteria, APs are secreted to the periplasmic space where they are believed to act mostly as phosphate scavengers. In one study, the volume and osmotic pressure of the periplasm were measured in different media for *E. coli* and *Salmonella typhimurium*. The results indicated that the ionic composition of the periplasm can differ from the external medium, especially in a medium of low ionic strength. The concentration of chloride was found to be around 200–400 mM inside the periplasmic space using a medium of approximately 100 mM ionic strength [9]. Furthermore, using a pH-sensitive green fluorescence protein variant (TorA-GFPmut3) fused to a periplasmic protein, the pH of the periplasm of *E.*

coli was found to equal the pH of the medium. Thus, pH is likely not regulated in the periplasmic space [10].

An AP from the Gram-negative, cold-adapted bacterium *Vibrio sp.* (VAP) is an interesting case, since it has been found very intolerant to heat at low ionic strength [11, 12]. Furthermore, VAP has been shown to be remarkably stabilized and activated by 0.5 M NaCl [12]. The mechanism for this ionic effect is unknown and was explored in the present study. Some APs are known to be activated by high ionic strength, such as the *E. coli* AP (ECAP) [13-15] and the AP from *Vibrio alginolyticus* [16]. The latter is closely related to VAP. Other APs, such as the human placental AP (PLAP) [17], are not activated by high ionic strength. The rate of phosphomonoester hydrolysis by APs increases with increasing pH, where the rate-limiting step becomes the release of the inorganic phosphate (P_2) from the phospho-enzyme complex at pH over 8.0 (Scheme 1). This pH dependence of the rate-limiting step causes a shift of the slowest step from dephosphorylation (k_3) to phosphate release (k_4) at higher pH [18]. Furthermore, the presence of a suitable phosphate acceptor, such as amine alcohols, provides competition for water as a nucleophile and speeds up the reaction rates.

Scheme I

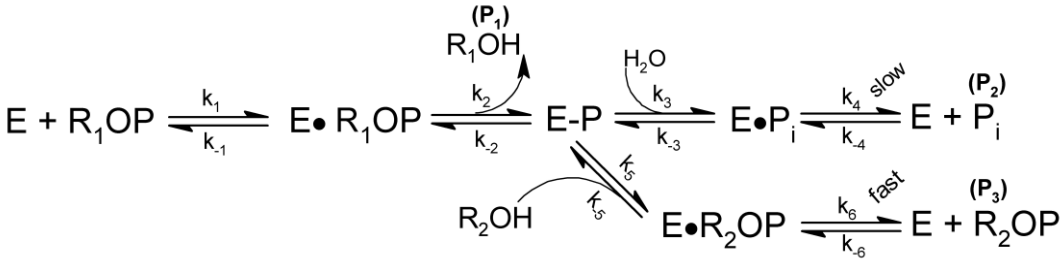

It has been postulated that ionic strength decreases the affinity of the enzyme for the phosphate product, leading to the increased rate of phosphate release (k_4). This has been directly measured by an increase in the inhibition constant (K_i) with inorganic phosphate at high ionic strength, where the dephosphorylation rate of E-P is only marginally affected by ionic strength [15]. Another aspect is the possibility that the ionic strength might be affecting rate-limiting

conformational changes. A conformational change of AP between active and inactive states has been postulated in older reports [19, 20] and asymmetric binding of phosphate or substrate has been directly observed for ECAP [21, 22]. The reaction cycle in the dimeric enzyme is believed to be half-of-sites in nature, where a conformational change between low and high affinity for the substrate is the driving force for catalysis by facilitating release of the product [22]. It is not fully understood how pH affects catalysis for APs and why some APs are not affected by ionic strength. In this study, we sought to answer how ionic strength influences the chemical and physical properties of VAP and, more specifically, how anions affect both the activity and stability. Furthermore, we wanted to answer how and why the enzyme is deactivated at a moderate temperature at low ionic strength.

Our results indicate that anions, rather than cations, both activate and stabilize VAP. The ionic effect was shown to be pH-dependent. The pH activity curves had two maxima, which is unique among APs, and that we propose is caused by a conformational change involving a deprotonation event in the pH range 9.0–10.5. Conformational changes were detected using tryptophan fluorescence which correlated with changes in activity and phosphate binding. Both NaCl and pH were further shown to affect the monomer/dimer equilibrium, suggesting their involvement in a conformational change. Interestingly, the drop in enzyme activity was not linked to dimer dissociation or metal ion depletion from the active site.

Materials and methods.

Materials. Chemicals were obtained from Sigma-Aldrich (Schnelldorf, Germany) or Merck (Darmstadt, Germany) unless stated otherwise. L-rhamnose and isopropyl β-D-1-thiogalactopyranoside (IPTG) were obtained from AppliChem (Germany). Bacto yeast extract and Bacto tryptone were purchased from Becton, Dickinson, and company (France). Triton X-100 was obtained from BPH chemicals (England) and chloramphenicol from Ampresco (USA).

Primers were obtained from TAG (Copenhagen, Denmark), Phusion polymerase from NEB (UK) and DpnI from Fermentas (Germany). Alkaline phosphatase from *E. coli* and calf intestines were purchased from Sigma-Aldrich.

Sub-cloning of VAP gene to pET11a. The VAP gene containing the original N-terminal export sequence (MKPIVTAVVTSTLSFNVLS) previously generated with a StrepTag II (WSHPQFEK) at the C-terminus [12], was sub-cloned from the pASK3-plus StrepTag vector (IBA, Gottingen, Germany) to a pET11a vector using the overlap extension PCR cloning method [23, 24]. Details of the cloning procedure can be found in the supporting information. Positive *E. coli* Top10 clones were selected and the plasmid subsequently purified on a GeneJET Plasmid Miniprep Kit (Fermentas, Lithuania) and sequenced (Genewiz, UK) to confirm 100% sequence identity. The VAP gene in the pET11a vector contained the StrepTag II sequence at the C-terminus with a two amino acid linker (Ser-Ala) between the polypeptide chain and the tag, upstream of the stop codon.

Enzyme expression and purification. *E. coli* Lemo21(DE3) cells (NEB, UK) were transformed with VAP-pET11a plasmid and clones selected on an LB-agar containing 100 µg/ml ampicillin and 30 µg/ml chloramphenicol. A single colony was inoculated to 20 ml of LB media starter culture containing 100 µg/ml ampicillin and 30 µg/ml chloramphenicol and shaken overnight at 300 rpm in a 100 ml Erlenmeyer flask at 37°C. The overnight culture was back diluted 1:100 fold into 200–250 ml of the same media containing an addition of 0.50 mM L-rhamnose and grown at room temperature in 1 L Erlenmeyer flask at 220 rpm until OD600 was 0.4–0.6, at which point the cells were induced by adding isopropyl β-D-1-thiogalactopyranoside (IPTG) to 400 µM. After induction, cells were grown at 18–20°C at 220 rpm until harvesting 16–18 h later by centrifugation. Cells were resuspended in 100 ml (1:10) lysis buffer (20 mM Tris, 10 mM $MgCl_2$, 0.1 % w/v Triton X-100, 0.1 mg/mL hen egg

lysozyme, 10 U/mL DNAse I [Sigma], pH 8.0) and incubated for 3–4 h at 4–8°C under gentle agitation and then quick-frozen under liquid N_2.

Purification of VAP, tagged with StrepTag, has been described elsewhere [12]. The active fractions of the elution peak were collected and analyzed for purity using SDS-PAGE (NuPAGE 4–20%) and then snap frozen in liquid N_2. The enzyme was not allowed to go through more than two freeze-thaw cycles before use in analyses. The snap freezing had no effect on the specific activity for a few freezing cycles if the enzyme was supplemented with at least 15% v/v ethylene glycol.

Standard activity assay. For standard activity assays, 10 µl of enzyme solution was mixed with 990 µl of reaction buffer (5 mM p-nitrophenyl phosphate, 1.0 M diethanolamine, 1 mM $MgCl_2$, pH 9.8) and the formation of p-nitrophenol (pNP) was monitored at 405 nm at 25 °C, using an extinction coefficient of 18.5 $mM^{-1}cm^{-1}$ for 30 s on a Peltier temperature-regulated Evolution 220 spectrophotometer at (Thermo Fisher).

Effect of ionic strength and pH on activity. Activity assays were performed under pseudo-zero order conditions ([S] close to V_{max}) using 5 mM p-nitrophenyl phosphate at 25°C unless stated otherwise. Salt solutions were added from 1.2–4.0 M stock (depending on the solubility of the respective salt species). Buffers were diluted to a final concentration of 50 mM from 0.2 M stock solutions. All buffers were titrated with HCl or NaOH to the respective target pH value. For pH dependence experiments, Mops was used as a buffer for pH 6.0–7.0, Tris for pH 7.0–9.0 and Caps for pH 9.0–11.5.

Ionic strength did not affect the measured pH values up to 1.0 M of the salt used. Furthermore, ionic strength did not greatly affect the molar extinction coefficient of pNP up to 1.0 M of salt. Of all the conditions tested, the molar extinction coefficient of pNP was only marginally affected by pH in the range used here (Figure S3). Thus, an average molar extinction

coefficient of 18.1 $mM^{-1}cm^{-1}$ was used for pH 8.0 measurements, 18.9 $mM^{-1}cm^{-1}$ for pH 9.0 and 19.0 $mM^{-1}cm^{-1}$ for pH 10.5.

Enzyme kinetics and competitive inhibition measurements. Enzyme kinetics were performed at 25°C for pNPP concentrations ranging from 0.0–2.0 mM at pH 8.0, 9.0 and 10.5 using 50 mM Tris for pH 8.0–9.0 and 50 mM Caps for pH 10.5. NaCl was added from 3.0 M stock solution and mixed with respective buffer diluted from 0.2 M stock solution. In the case where 1.0 M Tris or 1.0 M diethanolamine (DEA) were used, no additional buffer was added, and the pH titrated to the respective value used in the experiments. For addition of 1.0 M Tris or diethanolamine, the total ionic strength was set to 0.59 M by adding NaCl.

For K_i measurements, inorganic phosphate was added from a 100 mM Na_2PO_4 stock. The enzyme solution was diluted to 0.05–0.10 mg/ml, 10 µl solution mixed with 990 µl of buffer and A_{405} assayed for 30 s at 23°C on a Peltier temperature-regulated Evolution 220 spectrophotometer (Thermo Fisher). For exact determination of the p-nitrophenyl phosphate concentration, each sample was allowed to hydrolyze fully and the concentration determined by measuring the absorbance at 405 nm using the appropriate extinction coefficient. K_M and V_{max} were determined by non-linear regression fit to the Michaelis-Menten equation using the program GraphPad Prism. To evaluate k_{cat} ($k_{cat} = V_{max}/[E]_t$), the enzyme concentration was measured at A_{280} nm using a calculated molar extinction coefficient of 61310 $M^{-1}cm^{-1}$ for each monomer as described by Pace et al. [25].

The competitive inhibitor constant K_i for inorganic phosphate (PO_4^{2-}) was determined by global non-linear regression fit to $Y = V_{max}[S]/(K_M (1+[I]/K_i + [S])$, where Y is activity, [S] is the substrate concentration and [I] is the inhibitor concentration, using Graphpad Prism. The fit was applied to 0 mM, 0.5 mM, and 1.0 mM PO_4^{2-}.

Effect of sucrose on activity. For sucrose experiments and enzyme dilutions studies, the enzyme activity assays were performed on a SpectraMax 2 (Molecular Probes) plate reader by

monitoring the formation of pNP at 450 nm for 10–30 min (depending on enzyme concentration), or until the absorbance reached 0.4–0.5. All plate reads were done in 96-well plates, in duplicates or triplicates at ambient room temperature. The wavelength of 450 nm was chosen to keep the absorbance change during the reaction inside the linear range.

For sucrose experiments, the enzyme was diluted in 4×buffer concentration (0.20 M) and 50 µl mixed with 150 µl of 6.7 mM p-nitrophenyl phosphate, giving a final concentration of 5 mM and a respective final concentration of NaCl, sucrose (diluted from 4× stock) or nucleophile (Tris, diethanolamine) as denoted for each experiment.

Enzymatic assays after dilution. For enzyme dilution studies, the enzyme was incubated in 50 mM Tris buffer at pH 8.0–9.0 and 50 mM Caps for pH 10.5, starting from 2.15 µM enzyme stock solution (measured at 280 nm using an extinction coefficient of 122620 $M^{-1}cm^{-1}$ for dimer). Inorganic phosphate was added from a 100 mM stock solution and NaCl from a 3.0 M stock solution where indicated. The enzyme was serially diluted from a 0.015–0.50 µM enzyme solution (dimer concentration) by diluting 650 µl of the sample to 350 µl of the same buffer. Samples were incubated for 18–20 h at 25°C. The activity was then assayed at 25°C by mixing 180 µl of enzyme sample to 20 µl of aqueous 50 mM pNPP substrate solution. This 10% enzyme dilution, upon assaying, did not affect the outcome of the experiments since it was found that the rate towards enzyme dissociation equilibrium is reached within several hours.

Inorganic phosphate assay. Phosphate release during enzyme turnover (P_2) was measured using the PiPer phosphate assay kit (Thermo Fisher) following the manufacturers protocol for inorganic phosphate assay. An end-point analysis was performed at five different time points during the enzyme reaction under the same conditions as for the enzyme pNPP kinetic assay. No more than 10% of the substrate was allowed to hydrolyze during the time course to guarantee initial rate conditions. The rate of pNP release was also monitored for the same assay batch under identical conditions for comparison. At the defined time points, the enzyme

reaction was stopped by pipetting 100 µl of enzyme sample to 100 µl of 10 mM EDTA solution (pH 8.0) previously warmed to 90°C and kept at 90°C for 5 min before putting the samples on ice. The samples were then frozen at -20°C until further analysis. The typical inactivation method using 5% trichloracetic acid to stop the enzyme reaction was shown to affect the formation of the fluorescent product resorufin in the phosphate assay (data not shown), whereas EDTA had no effect (at the concentration tested in the assay). All samples were diluted 10× to a black, clear bottomed 96-well plate in 1× reaction buffer (0.1 M Tris, pH 7.5) to a final volume of 50 µl and then 50 µl of working reaction solution was added (100 µM Amplex Red reagent, 4 U/mL maltose phosphorylase, 0.4 mM maltose, 2 U/mL glucose oxidase and 0.4 U/mL horseradish peroxidase) and incubated for 45 min at 37°C.

Fluorescence was monitored on a Spectramax M3 (Molecular Probes) fluorescence plate reader using 530 nm for excitation and 590 nm for emission wavelengths in top read mode and an average read of 12 flashes. A standard curve was generated from the provided phosphate standard diluted in 1× reaction buffer in the range 0–50 µM phosphate. A blank was subtracted (1× reaction buffer) from all samples. By plotting the phosphate concentration vs. time, the initial slope of linear regression fit gave the initial rate of phosphate formation.

Enzyme thermal stability measurements. Thermal inactivation experiments were conducted in a digitally regulated heat-block using a heat-probe for accurate temperature measurements. The enzyme was diluted 100-fold to 500–1000 µl of buffer with various added ions giving a solution with enzyme content of ~10 U/ml and allowed to incubate for 60–120 s before starting the assay by pipetting 10 µl of enzyme sample to 990 µl of standard assay buffer (5 mM pNPP, 1 M diethanolamine, 1 mM $MgCl_2$, pH 9.8 at 25°C) and collecting at least five data points until the activity had fallen to 20–30% of initial activity. The rate of inactivation was determined by plotting ln(activity) vs. time, where the slope gives the rate constant, k of inactivation. The half-life was when calculated using the relationship $t_{1/2} = 0.693/k$.

For Arrhenius plots and $T_{50\%}$ determinations, five temperature points were measured at approximately $T_{50\%} \pm 5$°C. From an Arrhenius plot (lnk vs. 1/T), the activation energy (E_a) was obtained. $T_{50\%}$ was then calculated from the Arrhenius equation, where the k for 50% loss of activity after 30 min was used in each case (k = ln 2/30 min × 60 s/min^{-1}) to give $T_{50\%} = (E_a \times 1000)/R(\ln A - \ln k)$.

The thermal denaturation midpoint measurements (T_m) were determined in 25 mM Mops, 1 mM $MgSO_4$, pH 8.0 using circular dichroism (CD) in a 2-mm cuvette at 222 nm over the temperature range 15–90°C with a rise in temperature of 1 °C/min. Enzyme concentration was ~ 0.2–0.3 mg/ml. For monomer unfolding, a two-state pathway was assumed (N → U, where N is native, and U is unfolded). T_m was determined by a direct fit to a normalized sigmoid curve using the program GraphPad Prism.

Sample preparation for metal ion assay. Lemo21(DE3) *E. coli* cells, transformed with VAP-pET11a plasmid, were cultivated in a total of 1.0 L LB medium. Purification was done as described above on columns using 6 ml of fresh StrepTactin resin except the lysis buffer contained 100× less $MgCl_2$ (0.1 mM). The column was washed extensively with Chelex-treated 10 mM Tris, pH 8.0 buffer. Then, the resin was divided into two columns and 3 mL of either 0.1 M or 0.5 M NaCl in 10 mM Tris, pH 8.0 were added to each column and incubated at 37°C for 16 h under gentle agitation. The resin was then washed with 3 × 5 ml of Chelex-treated 10 mM Tris before the enzyme was eluted with 3 ml of Chelex-treated 15 mM desthiobiotin in 10 mM Tris pH 8.0 elution buffer. The eluted samples were then assayed for activity (see standard activity assay), protein concentration (A_{280}), and Zn^{2+}/Mg^{2+} content using atomic absorption spectroscopy (see below).

The metal-ion analysis was also done after incubating the enzyme, bound to StrepTactin, in urea. The resin was divided into four columns and incubated in 3 ml of 10 mM Tris, pH 8.0 buffer containing 0.0, 0.5, 1.2, or 2.0 M urea for 4 h at 4°C under gentle agitation (urea stock

solution was also Chelex-treated). The resin was then washed with 3 × 5 ml of Chelex-treated 10 mM Tris, the enzyme eluted and assayed as previously described.

Atomic absorption spectroscopy. Atomic absorption spectroscopy was performed on a Varian (Crawley, England) Spectra220 FS atomic absorption spectrometer. Standard curves for Mg^{2+} were made from 9949 Titrisol® (Merck) diluted to the range 0.00–1.00 mg/L in MQ-water and Zn^{2+} standards were made from 9953 Titrisol® (Merck) diluted to the range 0.00–1.00 mg/L in MilliQ-water. The measurement time was 1 s for each read and each measurement contained five reads for each of the standards and three reads for the samples. MilliQ-water was used as a blank for the standards and the elution buffer as a blank for the samples.

Tryptophan fluorescence measurements. Intrinsic tryptophan fluorescence was monitored at 20°C on a Fluromax 4P (Horiba) instrument using a 500-µl quartz cuvette with 4 mm path length. Enzyme sample from a 2.5 mg/ml stock was diluted to 0.040 mg/ml with a solution containing 1 mM $MgSO_4$ (for stabilization) and 50 mM buffer, using Mops for pH 6.0–7.0, Tris for pH 7.5–9.0 and Caps for pH 9.5–11.5. Slits were set to 3 nm and 5 nm for excitation and emission, respectively, using 295 nm for excitation, recording emission from 310–450 nm in 0.5 nm increments. The wavelength of maximum emission (λ_{max}) was determined mathematically using Excel Solver (LINEST function) by fitting the spectra from 320–380 nm with a third-degree polynomial ($y = ax^3 + bx^2 + cx + d$, where y is intensity and x is wavelength). By solving the roots for the first derivative of the equation, λ_{max} was determined.

Results

Activation of VAP by salt. Since we have previously observed both stabilizing and activation effects on VAP by using NaCl in the range below 0.5 M [12], we sought to study in detail the effect of various ions on the enzyme's structure, stability and function. First, we wanted to determine if the effect was specific for a particular type of ion(s) or followed the Hofmeister series effect [26, 27]. Figure 1A shows the effect of chloride salts and Figure 1B the

effect of sodium salts on the activity at pH 9.8. VAP was activated similarly in the concentration range of 0.0–1.0 M using four different chloride salt species (Figure 1A) with a plateau observed at 50–60% increase in activity. Using the sodium salts of various anions, a difference in activation was seen. Glutamate is one of the main osmolytes in *E. coli* and has been shown to be highly kosmotropic (ranks between F^- and SO_4^{2-}) [28]. Thus, we decided it would be an interesting comparison with inorganic ions. Sodium glutamate was, in fact, the most effective additive we tested in promoting the activity of VAP at ionic strength in the range 0–200 mM. However, at higher concentrations of glutamate, the activity dropped sharply. Sodium acetate, sodium nitrate, and sodium fluoride were all less effective than the chloride salts in activating the enzyme. At concentrations above 300 mM, fluoride stimulation reached a plateau similar to the chloride salts, whereas the activity diminished in the presence of acetate or nitrate. It may be concluded that ionic strength rather than the type of anion governed the salt activation of VAP at low salt concentration (0–200 mM), whereas, at higher concentrations of salt, an anion-dependent inhibition was produced by some of the anion types. Chloride and fluoride were not inhibitory to VAP, whereas glutamate, acetate, and nitrate did inhibit VAP.

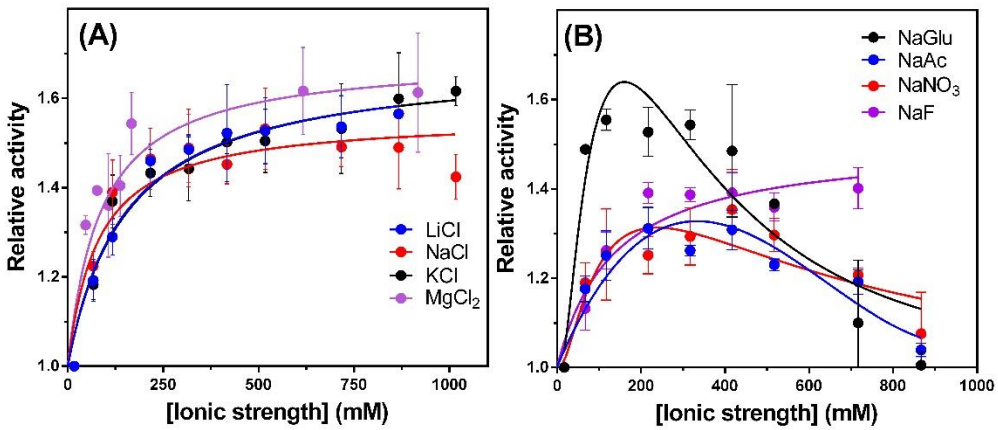

Figure 1. Salt activation of VAP at pH 9.8. (A) Effect of chloride salts and (B) sodium salts on activity. Activity was measured for pNPP hydrolysis in 50 mM Caps, 5 mM pNPP, pH 9.8 at 25°C. Data points were normalized to activity measured with no salt added. Data was fitted to hyperbolic function ($y = 1 + B_{max} \times x/(K_D + x)$) or log-Gaussian- function (y = 1 + amplitude × exp (0.5 × (ln(X/center)/width)^2) which fitted best, only to aid the eye. Measurements consisted of several independent experiments where activity was measured in duplicates (n = 2-5).

VAP activation by NaCl is dependent on pH. The activity of VAP with pNPP was measured in the pH range 7.0–10.5 with NaCl concentration ranging from 0.0–1.0 M (Figure 2A). The relative increase in activity induced by NaCl addition was 4-fold greater at pH 7.0–8.0 than at pH 9.8 (typical assay conditions). Changing the pH from 8.0 to 10.5 gradually decreased the ionic effect to near no effect at pH 10.5. The dependence of activity as a function of [NaCl] followed a hyperbolic dependence. By fitting the data to a hyperbolic equation for each pH, two coefficients could be derived. One is the I_{max} salt coefficient, which denotes the maximum activation induced by NaCl at the respective pH. The second is $I_{1/2}$, the salt activation coefficient, which is the concentration of salt needed to reach half I_{max} at the respective pH.

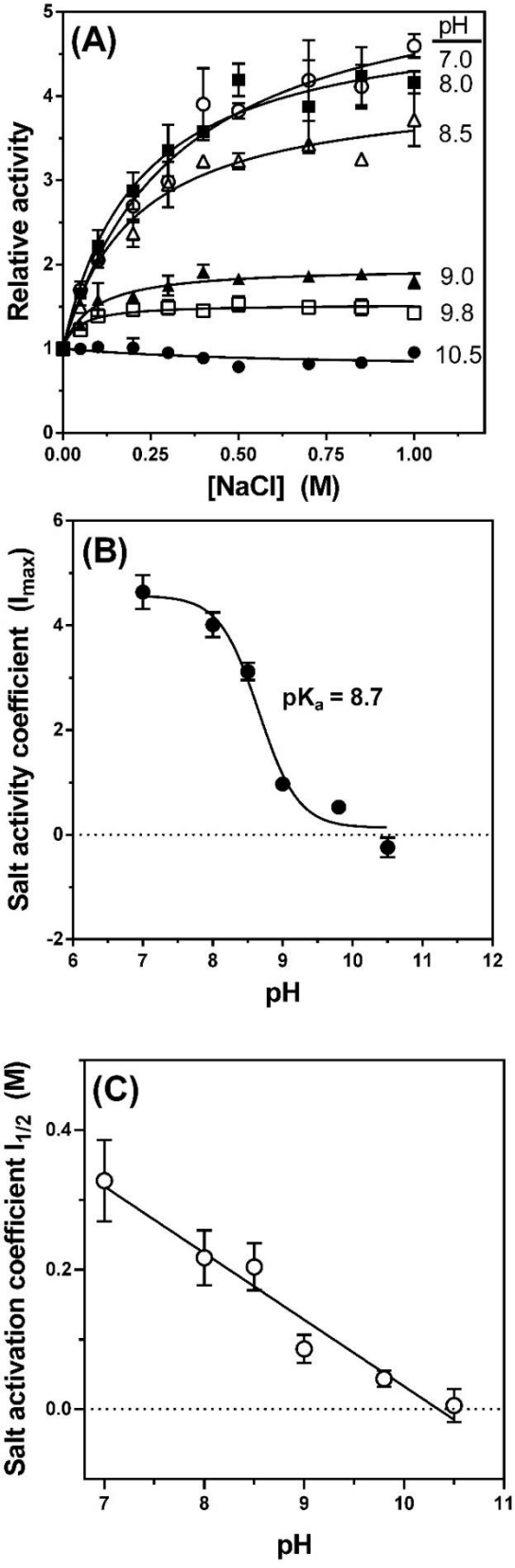
(A)
pH
7.0
8.0
8.5
9.0
9.8
10.5
Relative activity
[NaCl] (M)
(B)
pK$_a$ = 8.7
Salt activity coefficient (I$_{max}$)
pH
(C)
Salt activation coefficient I$_{1/2}$ (M)
pH

Figure 2. Effect of pH on NaCl activation for VAP. (A) Activity as a function of NaCl concentration. Activity was normalized at each pH value to activity measured with no NaCl added. Data were fitted to a hyperbolic function ($y = 1 + I_{max} \times x/(I_{1/2} + x)$) where y is activity, x salt concentration, I_{max} the salt coefficient, and $I_{1/2}$ the salt activation constant. (B) Salt coefficient I_{max} as a function of pH. Data were fitted with a variable slope sigmoidal curve (GraphPad Prism). (C) Near-linear relationship of salt activity constant $I_{1/2}$ as a function of pH in the pH range 7.0–10.5. Data consisted of several independent experiments where activity was measured in duplicates (n = 2–4).

The dependence of I_{max} on pH in the range 7.0–10.5 gave a sigmoidal curve, which is an indication of the enzyme occupying two states in this pH range (Figure 2B). One form that was activated by NaCl and another that is not affected by NaCl. The pK_a of a group responsible for the transition between the two states was found to be 8.7 under the conditions tested. Interestingly, the $I_{1/2}$ constant showed near-linear negative dependence on pH in the range 7.0–10.5. Thus, as the pH increased the enzyme was less activated by e.g. [NaCl] above 100 mM, and required less salt to reach the respective maximum activity attainable through NaCl activation. NaCl had no effect on the activity of VAP once the pH reached 10.5.

The pH activity profile of VAP gave two maxima. To better understand the salt activation of VAP, the pH activity profile was measured from pH 6.0–11.5, without adding salt (control) and after 500 mM NaCl addition (Figure 3A).

The pH activity profile showed two maxima at approximately pH 9.0 and 10.2. The addition of 500 mM NaCl increased the activity at pH 9.0 considerably but had hardly any effect on the maximum at 10.2. At pH 10.5, NaCl greatly increased the K_M for pNPP (see in Table S2) to such an extent that the concentration of substrate used was not enough to achieve V_{max}. Thus, the second maximum was slightly shifted towards a lower pH value using 500 mM NaCl.

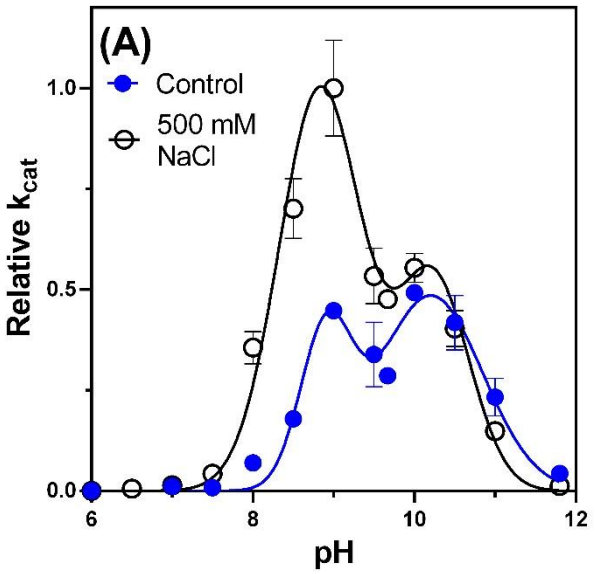
(A)
Control
500 mM NaCl
Relative k_{cat}
1.0
0.5
0.0
6
8
10
12
pH

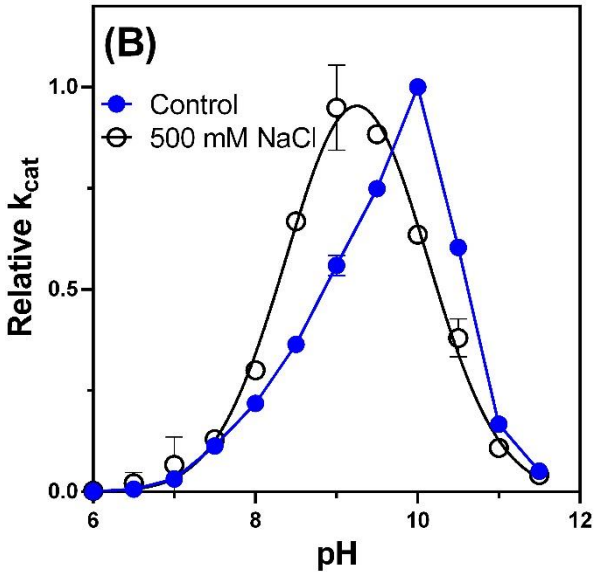
(B)
Control
500 mM NaCl
Relative k_{cat}
1.0
0.5
0.0
6
8
10
12
pH

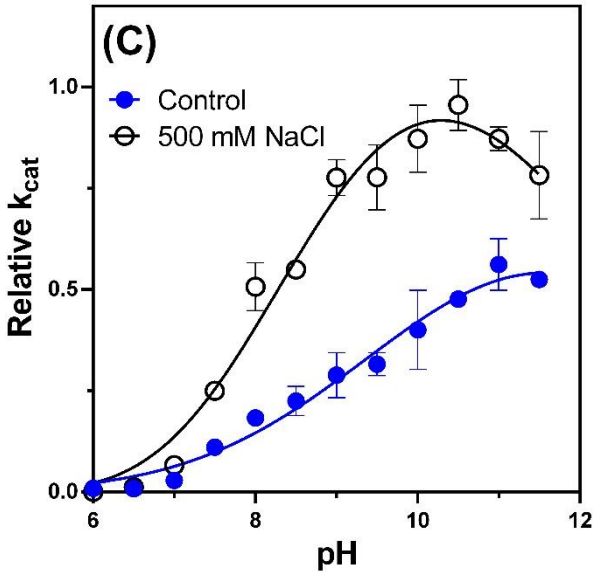
(C)
Control
500 mM NaCl
Relative k_{cat}
1.0
0.5
0.0
6
8
10
12
pH

Figure 3. Activity profiles as a function of pH for three alkaline phosphatases: (A) VAP, (B) Calf intestinal alkaline phosphatase, and (C) *E. coli* alkaline phosphatase. The pH activity profiles were measured either without any addition (control) or with 500 mM NaCl. Activity was normalized to the highest k_{cat} point measured for each enzyme activity profile. To aid the eye, curves were fitted with Gaussian, the sum of two Gaussian or Lorentzian functions, whichever gave the best fit. Data consisted of several independent experiments where activity was measured in duplicates (n = 2–4).

To address if these two maxima and the specific ionic activation around pH 9.0 for VAP were due to a systematic assay error, or substrate activation, and thus not a unique property of VAP, calf intestinal alkaline phosphatase (CIP) and *E. coli* alkaline phosphatase (ECAP) activity profiles were measured using the same conditions as used for VAP (Figure 3B, C). Only one pH maximum was observed for both CIP and ECAP. CIP was not activated by NaCl in agreement with previous observations [29]. However, the pH optimum shifted from pH 10.0 to pH 9.5 in 500 mM NaCl, possibly by affecting activity coefficients for pK_a values of groups responsible for activity (Debye–Hückel).

The activity of ECAP is known to be influenced by ionic strength [13, 30]. Here, NaCl was shown to increase the activity of ECAP at all pH values tested from pH 6.0–11.5. Furthermore, the pH optimum of ECAP was lowered by two pH-units in the presence of NaCl.

Effect of pH, ionic strength, and transphosphorylation on VAP enzyme kinetics. To study further the effect of pH, ionic strength and the presence of a transphosphorylation substrate on VAP activity, Michaelis-Menten kinetics were measured, as well as a competitive inhibition assay with inorganic phosphate, at pH 8.0, 9.0, and 10.5, together with the addition of 0.5 M NaCl or 1.0 M nucleophilic phosphate acceptor (Table S2).

The stimulating effect of NaCl on k_{cat} was pH dependent. Only the peak in Figure 3A at pH 9.0 was sensitive to NaCl while the other peak at pH 10-10.5 was not. Further analysis showed

that the affinity for substrate and product was greatly reduced at pH 10.5 (both K_M and K_i increased) while k_{cat} was unchanged by NaCl. In the presence of an organic phosphate acceptor (Tris or DEA), both k_{cat} and K_M were greatly increased. In most cases, the addition of 20% w/v sucrose decreased the activity substantially, indicating that the release of the inorganic phosphate product was the rate-limiting step at pH 8.0 and pH 9.0. At pH 10.5, sucrose had less effect on $k_{cat,}$ and by adding 0.5 M NaCl, sucrose had no effect on activity, indicating a possible shift in the rate-limiting step towards a step not affected by diffusion rates.

Thermal inactivation and denaturation of VAP are affected by ionic strength and pH. Inorganic phosphate or sulfate are well documented competitive inhibitors of AP activity [31-33]. Phosphate binds approximately ten-times more tightly to VAP than sulfate and provides much more protection against thermal inactivation than sulfate does. Figure 4A shows that VAP had a half-life of less than 1 min when heated at 30°C with no additional ions in the buffer. The half-life at 30°C increased to ~10 min and 50 min for 1 mM sulfate and 1 mM phosphate, respectively (Figure 4A). The cation added with the sulfate salts had no effect on VAP stabilization. Magnesium ions added as a chloride salt did not provide any specific stabilization and performed equally well as NaCl.

The effect of NaCl on thermal inactivation of VAP was further studied at 55°C in the range 0.0–1.0 M NaCl (Figure 4B). The half-life (for activity) at 55°C increased from 0.2 min to 38.5 min for 0.0 M NaCl and 1.0 M NaCl, respectively. It was noted that the rate of inactivation at 55°C did not decrease linearly with [NaCl] (Figure 4C), which is possibly due to thermal denaturation occurring when the temperature rises above 54°C and a stability plateau is reached. Figure 4D shows that NaCl increased the thermal midpoint for unfolding from 54.2°C to 62.2 °C when brought to 1.0 M NaCl, and the increase was linear with [NaCl] (Figure 4E). The thermal denaturation curves using CD showed that, upon the addition of NaCl from zero to 0.1 M, there was an increase in cooperativity for unfolding (steeper slope between the transition).

This cooperativity might be due to a chloride ion binding to a high-affinity site of as yet unknown identity.

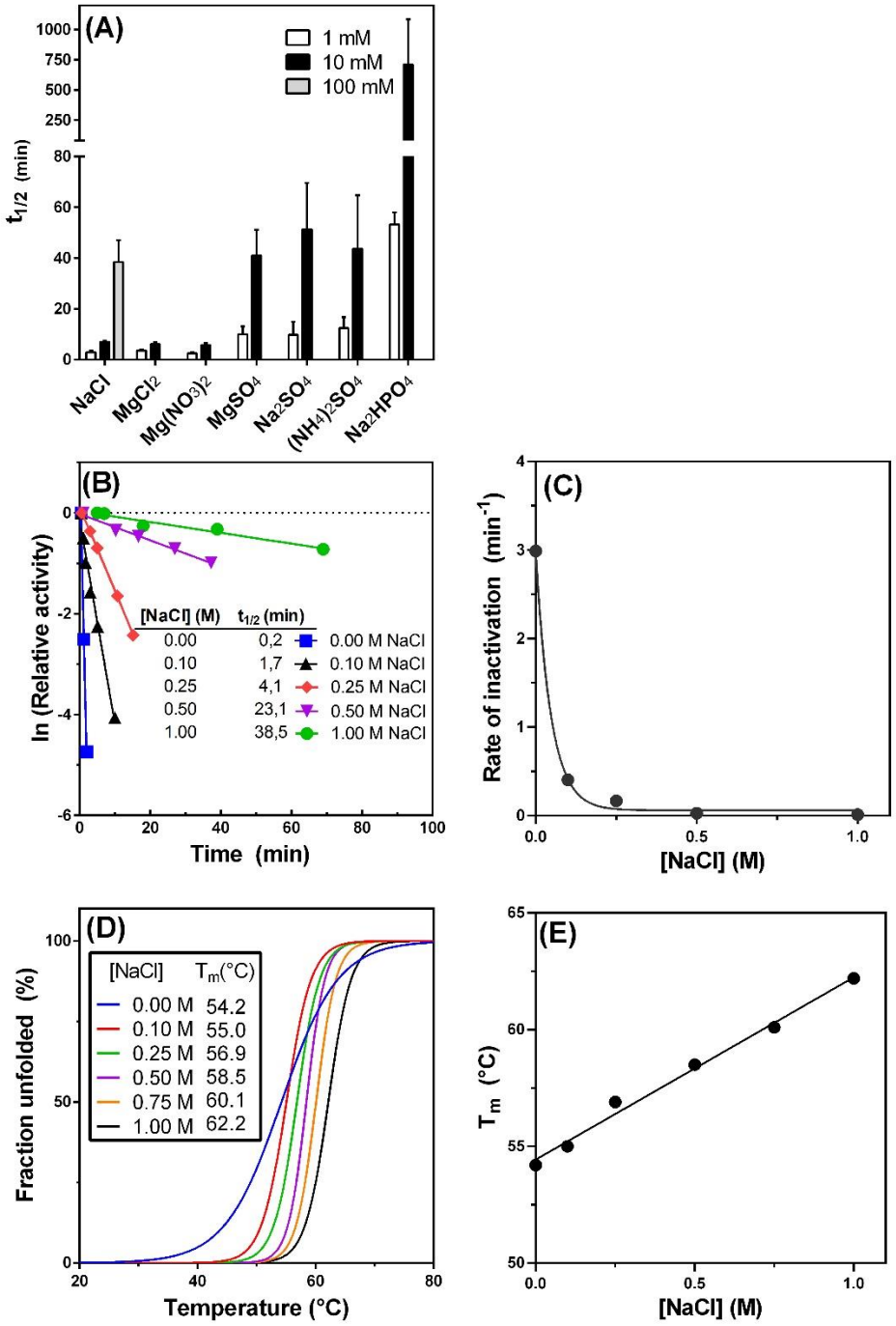

Figure 4. The effect of ions on VAP thermal stability. (A) The effect of NaCl, magnesium- and competitive inhibitor salts on stability at 30°C in 20 mM Tris pH 8.0. Aliquots of enzyme

were taken at different time points and assayed using the standard activity assay, and the half-life at 30°C ($t_{1/2}$) determined. (B) The rate of inactivation at 55°C vs. NaCl concentration in 20 mM Tris, 10 mM $MgCl_2$, pH 8.0. (C) The rate of inactivation at 55°C (k) as a function of [NaCl] using the data from (B). (D) Thermal denaturation of VAP vs. [NaCl]. The fraction of folded VAP was determined using CD-spectroscopy at 222 nm in 25 mM Mops, 1 mM $MgSO_4$, pH 8.0. The traces were normalized and fitted to a sigmoidal variable slope equation using GraphPad Prism. (E) The Linear dependence of T_m with NaCl concentration using the data from (D).

The linear dependence of NaCl on stabilization of the folded state observed here is likely due to salting-out effects of the denatured state, as is observed for many proteins [34]. However, it is unclear how salt affects the stabilization of the structural form with maximal activity. Table 1 shows the effect of 0.50 M NaCl on $T_{50\%}$. It can be seen that the effect of NaCl was pH dependent. At pH 8.0 the $T_{50\%}$ was greatly increased, from 25.8°C to 53.5 °C, for the control and 0.50 M NaCl respectively. Increasing the pH to 9.0 increased the thermal resistance of VAP as the $T_{50\%}$ rose to 30.6°C for the control. On the contrary, the effect of NaCl diminished where $T_{50\%}$ with 0.50 M NaCl was 50.5 °C at pH 9.0. At pH 10.5 the $T_{50\%}$ had increased to 33.2°C, but NaCl had no stabilizing effect at pH 10.5.

Table 1. The effect of sodium chloride on thermal inactivation.

pH	$T_{50\%}$ (°C)[a] Control	$T_{50\%}$ (°C)[a] 0.50 M NaCl
8.0	25.8 ± 1.4	53.5 ± 1.5
9.0	30.6 ± 0.6	50.5 ± 0.5
10.5	33.2 ± 1.0	31.7 ± 1.1

[a] Samples were incubated in 20 mM, Tris, 10 mM $MgCl_2$ at pH 8.0/pH 9.0 or 20 mM Caps, 10 mM $MgCl_2$ for pH 10.5 with or without the addition of 0.50 M NaCl on a heat-plate with time at various temperatures and the $T_{50\%}$ determined by assaying the remaining activity in the

standard assay at pH 9.8 and 25°C. The mean and standard deviations reflect 2-5 independent experiments.

The inactive state of VAP is dimeric and still contains Zn^{2+} and Mg^{2+}. We previously found that urea-induced inactivation of VAP produced an inactive dimeric state [12]. We sought to answer the question if the inactivation of the enzyme involved Zn^{2+} or Mg^{2+} dissociation. We expected that ion dissociation might accompany or be the main cause of inactivation. In particular, loss of the Mg^{2+} ion could result in failure to activate the nucleophilic Ser in the active site. Our VAP storage buffers contain a rather high concentration of $MgCl_2$ (10 mM) and, therefore, it has proven difficult to remove the extraneous Mg^{2+} sufficiently below the enzyme sample concentration (10-20 μM) by filtration or dialysis, without possibly promoting its dissociation from the active site. As mentioned above, the initial hypothesis was that inactivation observed in low-salt buffer solutions was due to dissociation of the Mg^{2+} from the active site. Thus, we reduced the Mg^{2+} content of the lysis buffer 100-fold (0.1 mM) and used Chelex-treated, 10 mM Tris buffer in all purification steps. Furthermore, the enzyme was immobilized on StrepTactin resin (Figure S4) and inactivated while still bound to the resin at 37°C for 16 h in 0.1 M NaCl or 0.5 M NaCl (Figure 5A). The latter condition prevents inactivation observed in buffers of low ionic strength and served as a control. At 37°C, 0.1 M NaCl was not enough to protect the enzyme against inactivation, the specific activity being 75% lower than in the sample with 0.5 M NaCl. There was not a statistically significant difference in the Mg^{2+} content of VAP treated in 0.1 M NaCl buffers (1.8 ± 0.4) compared with VAP when 0.5 M NaCl was present (1 ± 0.8). The high standard deviation is due to lower binding affinity of the StrepTag at 37°C compared to 4°C, especially for the 0.1 M NaCl sample leading to lower concentration of enzyme eluted, and thus higher signal to noise for both atomic absorption and protein concentration assay. Interestingly, there was a significant difference in Zn^{2+} content depending on salt concentration, being 2.0 ± 0.7 per monomer for 0.5 M NaCl and

1.0 ± 0.1 per monomer for 0.1 M NaCl. Thus, VAP lost one of its two Zn^{2+} ions when the NaCl concentration was dropped from 0.5 M to 0.1 M. However, the magnesium ion content was unchanged. It should be noted that due to loss of protein content from the columns under the latter condition, the reason for which is being looked into, the error in the data was relatively large.

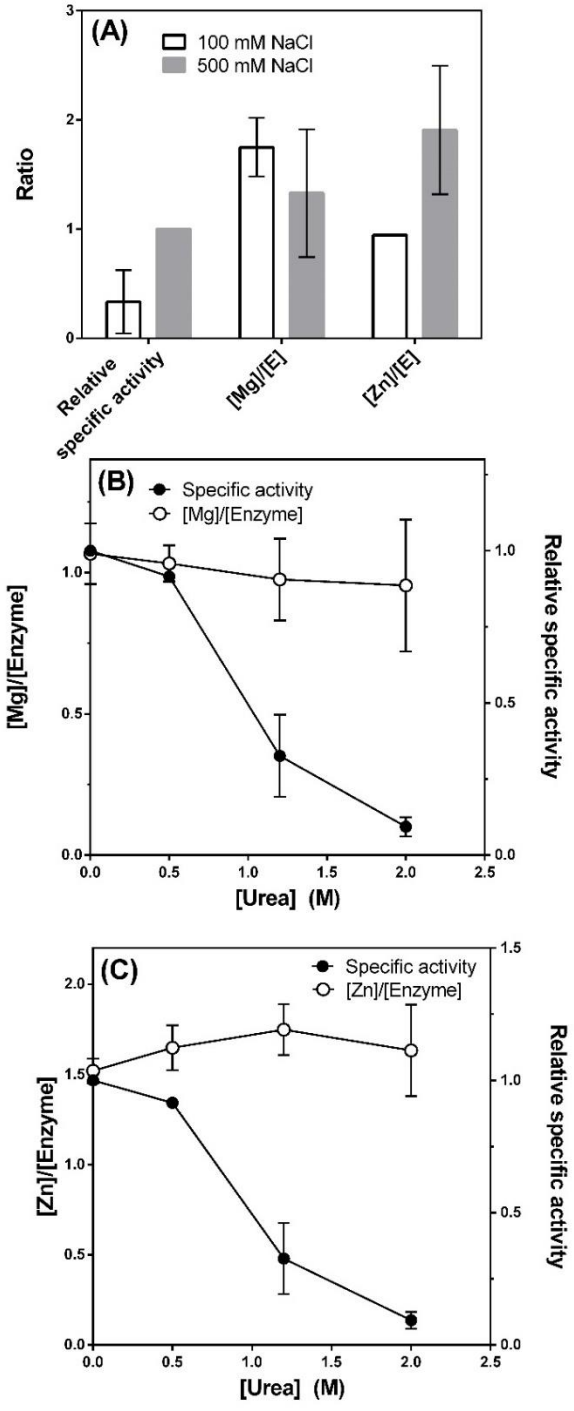

Figure 5. Determination of the Zn^{2+} and Mg^{2+} ion contents during VAP inactivation. (A) Zn^{2+} and Mg^{2+} contents were normalized to enzyme monomer concentration after thermal inactivation at 37°C for 16 h at pH 8.0 in the presence of 100 mM NaCl or 500 mM NaCl. (B) Mg^{2+} content, and (C) Zn^{2+} content of VAP after incubation of the enzyme in urea at pH 8.0 for 4 h at 4°C. Data were normalized to the enzyme monomer concentration. Means and standard deviations reflect several independent measurements (n = 2–5). Note that some error bars are smaller than the borders of the symbols or columns and, thus, are not visible.

After immobilization of the enzyme to the StrepTactin resin, we also applied the resin to four separate columns, and incubated the resins in 0.0-2.0 M urea for 4h. After rinsing with Chelex-treated Tris buffer, the enzyme was eluted as described above (Figure S4). The samples were then assayed for Mg^{2+} content (Figure 5B), Zn^{2+} content (Figure 5C) and specific activity. The inactivation occurred without changes in the metal content.

VAP adopts several structural states with respect to pH. It is unclear how many deprotonation events occurred in Figure 3A. If we assume each ascending and descending limb in the bell-shaped activity curve is due to a single protonation event, then there are possibly four deprotonation events that affect VAP activity. The second maximum might also be due to a conformational change resulting in a change in the rate-limiting step towards the hydrolysis step.

This would explain why salt had no effect on the second maximum, since dephosphorylation of the covalent intermediate, within the active site, would be minimally affected by the ionic strength. The activity presented on the y-axis in Figure 3B was assayed at saturating concentration of substrate (over 10-fold K_M). At pH above 10.0, the affinity for the product (measured as K_i) was greatly decreased. This is likely reflected in the second maximum at pH 10.2, since the release of the product is the rate-limiting step in the reaction pathway at alkaline pH. The limb of the second peak may decrease sharply with increasing pH (Figure 3) due to a

decrease in relative activity, since the activity measured no longer represented V_{max} (at 5 mM substrate) as K_M was also increasing as the pH rose from pH 10.0.

To address the question of whether pH changes might be inducing structural changes, we monitored tryptophan fluorescence for VAP under identical conditions as used in Figure 3. We used two fluorescence methods to represent the structural changes, (i) the absolute tryptophan fluorescence intensity at 340 nm (Figure 6A) and (ii) the wavelength of maximal fluorescence, λ_{max} (Figure 6B). The absolute intensity value (and the changes in intensity) is sensitive to the distance and orientation of electron-deficient residues in proximity to the indole group(s). On the other hand, the λ_{max} is more an indicator of solvent accessibility to the indole group(s), and not as sensitive to intrinsic quenching events. Three distinctive states could be detected from the absolute fluorescence intensity at 340 nm with changing pH. Figure 6A shows where fluorescence dropped between pH 8.0–9.0, correlating with activation of the enzyme (dotted lines are adopted from the activity profile in Figure 3 for comparison). Another drop in fluorescence was seen at pH 10.0–11.0, correlating with the large increase in K_M and K_i (Table 1). In the presence of 0.5 M NaCl, the trend in fluorescence was similar except the transition was shifted towards lower pH values. A similar shift was seen for the activity pH profile (Figure 3). The fluorescence at 0.5 M NaCl was also slightly lower for pH 10.0–11.5 than for the control.

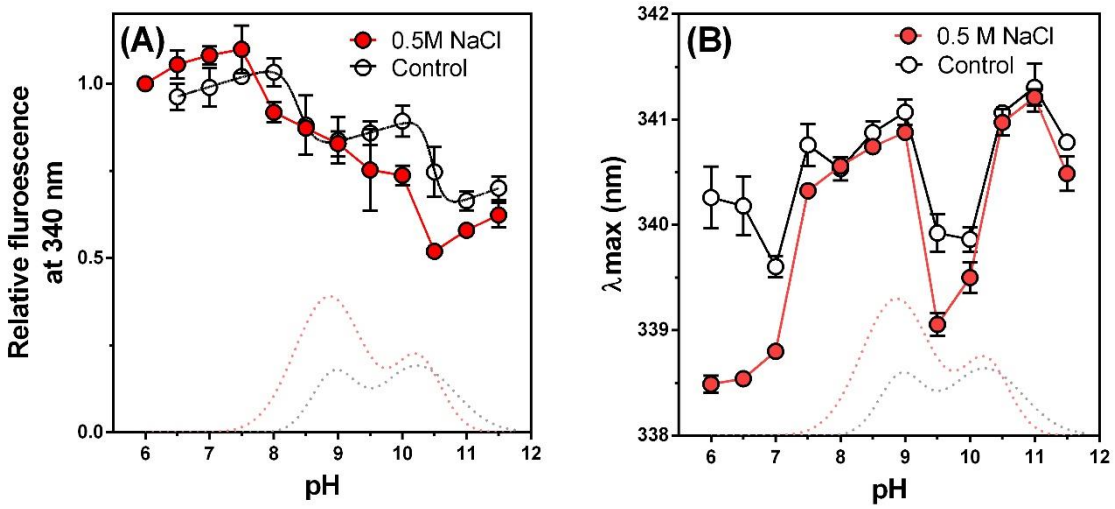

Figure 6. VAP tryptophan fluorescence as a function of pH. (A) Relative tryptophan emission at 340 nm as a function of pH. (B) The wavelength of maximum emission (λ_{max}) as a function of pH. The dotted line curve is adopted from VAP activity pH profiles in Figure 3A for control (black) and 0.5 M NaCl (red) for comparison.

The emission wavelength shift (Figure 6B) showed pH-dependant transitions in VAP structure presumably due to subtle changes in solvent accessibility of certain Trp residue(s). Four transitions were observed (between pH 7.0–8.0, 9.0-9.5, 10.0-10.5 and 11.0-11.5). The first transition did not correlate with any activity change but the second and third transitions did correlate with a decrease and subsequent increase in activity, respectively. Thus, they correlated well with the two maxima in Figure 3. The last transition correlated with the large increase in K_M and K_i that occurs when pH becomes high. Interestingly, the λ_{max} was quite different at pH 6.0 when 0.5 M NaCl was added, being 338.5 nm and 340.5 nm for 0.5 M NaCl and the control, respectively (Figure 6A). Apart from that, the λ_{max} followed the same trend as the control. Possibly the native fold is not as stable without NaCl present at pH 6.0–6.5 and is partially

unfolded, leading to a higher λ_{max} value. This would explain the drop in λ_{max} for the control going from pH 6.5 to 7.0.

Effect of buffer conditions on dimer-monomer equilibrium. We have observed an effect of NaCl on both the activity and thermal stability of the active site ($T_{50\%}$), as well as on the native fold (T_m). Since the monomers of APs are generally inactive, no information on the effect of ionic strength on the dimer-monomer equilibrium could be obtained from the earlier experiments. Therefore, we attempted to induce dissociation of dimers to monomers by dilution. The dimer to monomer dissociation was detected using specific activity of the enzyme.

It can be problematic to use the activity as a measurement if the K_d is high, due to difficulties of measuring the initial rate at high enzyme concentration. This problem can be overcome by assaying the activity by an additional dilution into a reaction buffer and assume the equilibrium does not shift during the assay (not a problem if dissociation rate is slow).

We performed dilution of VAP to test for dissociation and found dissociation occurring below 50 nM dimer. Instead of applying a further dilution to a reaction assay buffer, a concentrated solution of pNPP was mixed with the samples to a final concentration of 5.0 mM to initiate the activity assay, thus resulting only in an additional 10% dilution.

The rate of dissociation was measured by dilution at pH 8.0 using different initial concentrations of VAP (Figure 7A–C). Equilibrium was reached in approximately 8–10 h. The rates of dissociation at 15 nM dimer were 0.004 and 0.003 min^{-1} in buffer containing 1 mM inorganic phosphate or 0.50 M NaCl respectively. Without these stabilizing additives, the activity of the enzyme fell too quickly to reflect the state of the dimer-monomer equilibrium. To rule out that the enzyme concentration dependence of the specific activity was due to magnesium dissociation, the enzyme was diluted at 15 nM dimer with an addition of 10 mM $MgCl_2$ (Figure 7D). Magnesium did not affect the dissociation equilibrium.

The dimer dissociation constant, K_d, was derived by applying serial dilutions in the range 0–100 nM at pH 8.0 (Figure 7E) and pH 10.5 (Figure 7F) and the activity assayed 18 h later. It can be seen that phosphate ions increased the K_d from 7.3 ± 5.9 nM at pH 8.0 to 23 ± 7.5 nM for the control in the presence of 1 mM phosphate. Interestingly, at pH 8.0 using 0.50 M NaCl, the K_d increased to 20 ± 8.6 nM with a distinctive sigmoidal character (S-shaped curve) not seen at pH 10.5. Increasing the pH to 10.5, the K_d was greatly decreased to 0.4 ± 0.3 nM, where there was no significant difference for 1.0 mM P_i or 0.7 ± 0.2 nM. For 0.50 M NaCl at pH 10.5, the K_d was similar to values obtained at pH 8.0 or 11.1 ± 6.3 (Table 2).

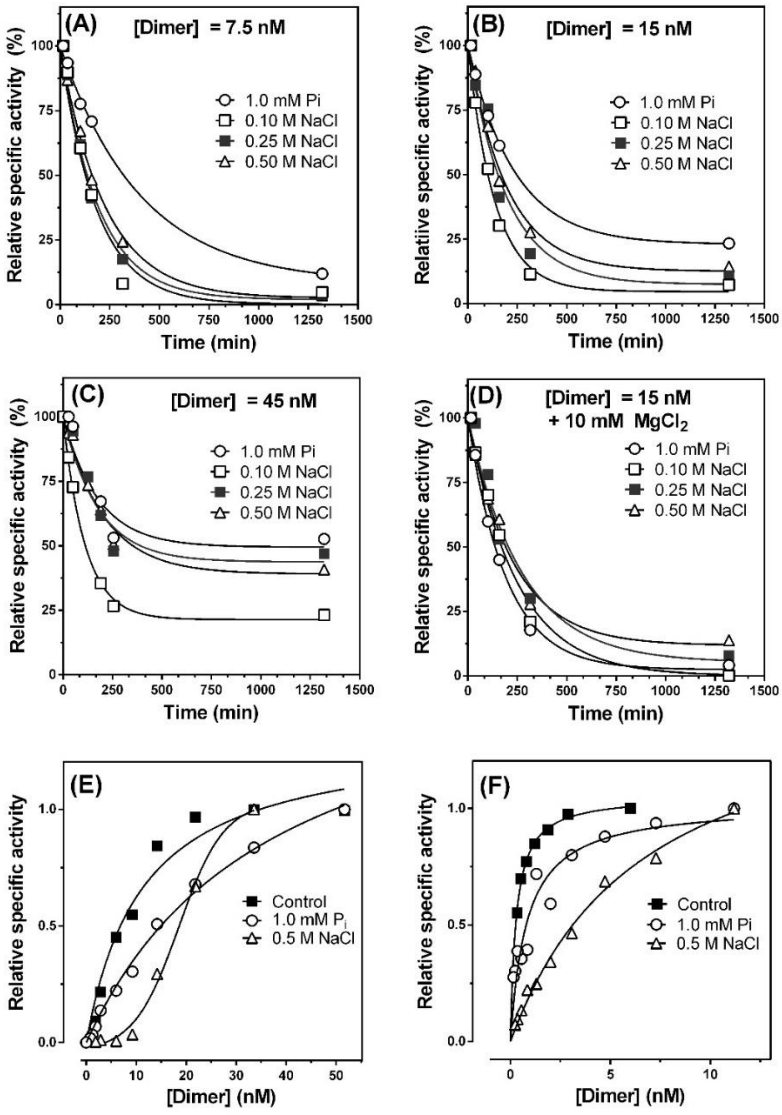

Figure 7. VAP dissociation induced by dilution. The rate of dissociation was determined as a function of enzyme concentration at pH 8.0 and 25°C for different initial concentrations: (A) 7.5 nM dimer, (B) 15 nM dimer, and (C) 45 nM dimer. (D) The effect of magnesium was tested by incubating 15 nM dimer (as in B) in 10 mM $MgCl_2$. (E, F) Examples of enzyme dilution curves used for K_d analysis (summarized in Table 2) at pH 8.0 (E) and pH 10.5 (F) after 18 h incubation. Curves in (A–D) were fitted to a single exponent decay function, and curves in (E, F) were fitted to a one-site binding hyperbola except for 0.5 M NaCl addition at pH 8.0 a sigmoidal fit was applied.

The stability of the dimer was shown to be relatively high with dimer dissociation free energy in the range of 40–50 kJ/mol. Thus, the reason(s) for VAP's low thermal resistance is not due to an unstable dimer but some other transition to an inactivated state which is not enzyme concentration dependent. Thermal inactivation at 25°C for VAP was not concentration dependent. This can be observed in the dilution experiments where absolute specific activity was much less for the control than when phosphate or NaCl was added. After 18 h incubation at 25°C, over 90% of the enzyme was inactivated. However, the remaining population of active enzyme residues was still affected by dilution. The thermal inactivation should not affect the K_d value obtained since only the remaining active dimer subunits are being measured relative to enzyme concentration. Adding 1.0 mM phosphate or 0.50 M NaCl protected the enzyme against thermal inactivation. Thus, thermal inactivation was not due to concentration-dependent dimer dissociation.

Table 2. The pH dependence of VAP dimer-monomer equilibrium.

pH 8.0[a]	**K_d**[c] **(nM)**	**ΔG_d**[d] **(kJ/mol)**
Control	7.3 ± 5.9	46 ± 2
1.0 mM P_i	23 ± 7.5	44 ± 1
0.50 M NaCl	20 ± 8.6	44 ± 1
pH 10.5[b]		
Control	0.4 ± 0.3	54 ± 2
1.0 mM P_i	0.7 ± 0.2	52 ± 1
0.50 M NaCl	11 ± 6.3	45 ± 1

[a] Samples were incubated for 18 h at 25°C and activity assays performed in 50 mM Tris, 5 mM pNPP at 25 °C

[b] Samples were incubated for 18 h at 25°C and activity assays performed in 50 mM Caps, 5 mM pNPP at 25 °C

[c] Data from Figure 7E and F was either fitted to a hyperbolic function: ν_{spec} = Top*[E]/(K_d + [E]), or a sigmoidal function: ν_{spec} = Bottom + (Top-Bottom)/(1+10^(log(K_d)*[E])*Hill-slope) where ν_{spec} is the specific activity, [E] is the enzyme dimer concentration, K_d is the dissociation constant, Top is the maximum specific activity, Bottom is the background specific activity and Hill-slope is the slope for the transition between the two states. The K_d constant represents the dissociation constant for the dimer species, $K_d = [M]^2/[D]$ where M denotes monomer and D the dimer.

Discussion

Effect of ions on VAP activation. It is well known that anions dominate the Hofmeister effect over cations for both stability and activity [35]. If the effects of chosen ions on VAP observed in this study were due to general solvent effects, then the anions should follow the Hofmeister sequence from being stabilizing/activating to being destabilizing/inhibitory as such: $Glu^- > F^- > CH_3COO^- > Cl^- > NO_3^-$, and the cations should follow the sequence $K^+ > Na^+ > Li^+ > Mg^{2+}$. The anionic effect seen here did not follow a typical Hofmeister series, making it unlikely that the ions were changing the VAP's behavior by affecting the solvent. More likely, the anions were interacting specifically with a charged residue on the protein surface, most likely near or in the active site.

There are many examples of ions not following the Hofmeister effect when affecting the function of enzymes, which is likely due to relevant positions of surface charges and polarity of the main chain in the folded protein [36, 37]. A good example is the fact that salting-out of

lysozyme only followed the Hofmeister series under high ionic strength or at alkaline pH. At acidic or neutral conditions, the Hofmeister series was reversed for lysozyme [38]. Another example was the reversing of Hofmeister series for the salting-out of the tripeptide GGG when the N-terminal amine was capped [6].

A study on ECAP activity using 17 chloride and sodium salts showed that the salt-induced activation followed mostly the Hofmeister series. The activation did not involve any structural changes, and the conclusion was that the ionic strength weakened the electrostatic interactions in substrate binding and product release [30]. Another study on calf intestinal alkaline phosphatase (CIP) showed a similar trend. Overall, for CIP the salts mostly affected K_M and the pH optimum (as observed in Figure 3B), but the V_{max} was only slightly affected.[39]

Dependence of VAP activity on pH and ionic strength. In the present work, we found that the activation by NaCl was highly pH-dependent (Figure 2 and 3), forming two maxima in the pH activity profile. It can be suggested that the enzyme may adopt two structural states, one that is affected by NaCl and the another which is not. Applying this assumption, a pK_a of 8.7 was derived from a deprotonation event (Figure 2B). It is possible that the chloride ions were directly involved in an ionic bond with a particular charged group in the first maximum that was being deprotonated in the second maximum. Else, the increase in the pH led to conformational change involving several residues which is affected by ionic strength. A direct binding of Cl^- to ECAP has been observed using ^{35}Cl NMR, where it was proposed that Cl^- might bind to a charged amino acid with a high exchange rate [40]. Another more detailed study, using both ^{35}Cl and ^{113}Cd NMR (by studying the Zn and Cd saturated enzyme respectively), showed that Cl^- binds to the Zn ion in the M1 site. The Zn ion had five ligands in the E-P state with three histidyl groups and either two Cl^- or two water molecules [41]. These authors also reported different affinities of the two monomers for phosphate ions, implying two different conformational states.

The candidate ionizable charged groups causing a change in activity in the pH range under study here would be His (pK_a 6.0), Lys (pK_a 10.5) or Arg (pK_a 12.5). Most of the titratable side chains in the active site of VAP take part in ligation of the metal ions. One candidate in VAP would be Arg129 that binds two of the non-bridging oxygens of the phosphate group in substrates. Other candidates would be Arg113, H465 or His277 or His116, the latter two being zinc binding histidyl ligands. However, even though pK_a values of amino acids can be offset by proximity to charged or polar groups, it is more likely that deprotonation of a hydrated metal ion is taking place as has been proposed for ECAP rather than involvement of these positively charged residues [41, 42].

O'Brian and Herschlag (2002) evaluated k_{cat}/K_M as a function of pH under pre-steady-state condition for ECAP using alkyl phosphate substrates, which have a poor leaving group [42]. The rate-limiting step over the pH range tested, for the alkyl phosphates, was the initial phosphorylation of the nucleophilic Ser. An ascending activity limb at around pH 5 was believed to be caused by deprotonation of the substrate mono-anion and the nucleophilic Ser in the active site. The descending limb was linked to the deprotonation of a Zn coordinated water molecule with a pK_a of 8.0, leading to inactivity. Under steady-state conditions, using pNPP as a substrate, the pK_a of the ascending limb for ECAP was reported to be in the pH-range of 7.1–7.4 [43, 44]. This was attributed to a basic group. However, the pK_a 8.6–9.2 of the descending limb was attributed to a deprotonation step of an acidic group involved in substrate binding (possibly a Zn-coordinated water molecule as previously discussed). In our hands, the pH optimum of ECAP under steady-state conditions was shifted towards a higher pH value by a factor of approximately 1.0 pH, compared to results in older reports [43, 44] (Figure 3B), although a similar "alkaline" pH optimum has previously been reported for ECAP [45]. The most probable explanation for this inconsistency is the different assay conditions used (buffer species and substrate concentration), and whether the pH optimum is reported using k_{cat} or k_{cat}/K_M. For

VAP, evaluation of V_{max} needed to be done at high substrate concentration since K_M was highly dependent on pH in the range 9-10.5.

By observing the kinetic data in Table S2, and comparing the kinetics for the control and the 0.5 M NaCl addition, NaCl had a different effect at pH 8.0 compared with pH 10.5. At pH 8.0, the K_M was not affected by NaCl, whereas K_i was increased 4-fold, which would fit the 4-fold increase in k_{cat} due to faster phosphate release (the rate-limiting step).

At pH 10.5 with 0.5 M NaCl, the K_M was 3.5-times higher than the control. The K_i was also increased by 6-fold for 0.5 M NaCl compared to the control. However, this increase in K_i induced by NaCl was not reflected in higher k_{cat}, indicating that the rate-limiting step was no longer the release of phosphate. This suggestion was supported by the fact that sucrose, used to increase the viscosity in the buffers, generally reduced activity. The activity observed at pH 10.5 in 20% w/v sucrose was 83% of the control with no sucrose added, whereas no effect on the activity was observed where both 0.5 M NaCl and 20% w/v sucrose was added. This suggested that at pH 10.5, the activity in 0.5 M NaCl was not affected by increasing the viscosity. It is also possible that viscosity could affect the rate of a conformational change, especially if the conformational change is entropy driven and involves the release of bound water molecules.

The following scenarios for VAP activation by ions in the pH range 8.0–10.0 VAP could be derived.

(1) Salt affects kinetics by allowing faster product release. This has been shown for ECAP [15, 30], and is likely also true for VAP. A possible explanation for the pH-dependence of salt activation for VAP, disappearing at more alkaline pH, would be that a conformational change occurs in VAP at around pH 10.0 and the release of the product is no longer rate-limiting. Then, the hydrolysis of the covalent intermediate would likely become the rate-limiting step (k_3) which would not be affected by the ionic strength of the medium. For ECAP, no comparable

conformational change occurs in this pH range, so that the ionic strength activation is not pH dependent.

(2) Salt affects conformational states. Some researchers have proposed two conformational states for ECAP when present as a covalently-bound phosphate complex (E-P), where one form of the enzyme is suitable for transphosphorylation and the other for hydrolysis [46]. Although suggestions of conformational changes as part of the reaction mechanism of ECAP and other APs have repeatedly been made, they have not been observed experimentally. Often, such theories have been linked with a half-of-sites reaction mechanism [19-22], where the binding affinity shifts reciprocally between subunits for substrate binding and product release. The putative conformational change suggested here for VAP could be a reflection of a half-of-sites structural dynamics. Changes in tryptophan fluorescence with pH correlated with changes in activity, possibly an indication of such conformational change. At pH 8.0, one subunit might have low affinity for substrate and inorganic phosphate (product) while the other subunit would have a high affinity for substrate (and product), and be catalytically efficient (Figure 8). In VAP, a conformational change during the reaction cycle might occur after the dephosphorylation reaction, but before the release of the phosphate ion, where the subunit switches between the states to release the phosphate. The rate-limiting step at pH 8.0 would be the phosphate product release (or possibly the conformational change) according to this scenario. At pH 10.5, both subunits might adopt the low-affinity state, where K_M and K_i are greatly increased with the consequence that the release of product is fast and the dephosphorylation rate slow and becomes the rate-limiting step. This kind of mechanism has recently been shown for fluoroacetate dehalogenase from *Rhodopseudomonas palustris* where only one subunit in the asymmetric homodimer underwent a catalytic turnover. The empty subunit took a role in allosteric communication between subunits where an entropy change due to a release of water molecules played a key role [47]. Molecular dynamics simulations of VAP have shown that the subunits are

asymmetric and are dynamically promiscuous, having different networks of ns-scale movements [48].

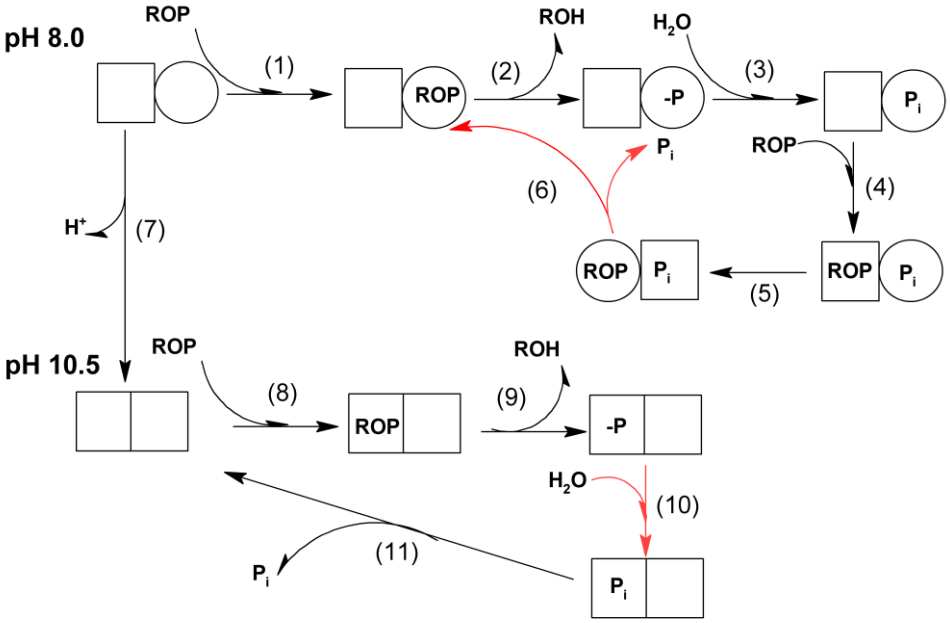

Figure 8. A hypothetical scheme for a half-of-sites reaction mechanism of VAP hydrolysis at pH 8.0 and pH 10.5 under saturating substrate concentration. Open circles denote a subunit with high affinity for both the substrate and phosphate product and the open square denote a subunit with low affinity for the substrate and phosphate product. At pH 8.0, the release of the phosphate product is the rate limiting step (step 6 depicted in red). Before phosphate release, a conformational change occurs where subunits switch between the low affinity and the high-affinity state (step 5). Increasing the pH to 10.5, results in conformational change triggered by a deprotonation event so that both subunits adopt the low-affinity state. Subsequently, phosphate release is faster, and the rate-limiting step becomes the dephosphorylation (step 10).

(3) Anions bind to a specific site in the active site of VAP. At a moderate concentration of salt and below pH 10.5, VAP activity increased, irrespective of the nature of the anion (Figure 1). Furthermore, the active site heat stability ($T_{50\%}$) increased with NaCl with a similar pH trend as for activity (Figure 4 and Table 2). A similar pH-dependant anionic activation as shown here

for VAP was previously described in a study on an AP from another marine bacterium, *Vibrio alginolyticus* [16]. VAP and *Vibrio alginolyticus* AP have 93% sequence identity and have identical active site residues with respect to metal ion coordination. Furthermore, they both have the same large surface loop insert, that was noted as a novel structural characteristic of VAP when its crystallographic structure was reported [49]. For *Vibrio alginolyticus* AP, Cl^- ions were shown to be most effective in enhancing enzyme activity compared to other small anions. However, SO_4^{2-}, a competitive inhibitor, was shown to prevent the effect of Cl^- on activity at pH 7.5. Thus, it was concluded that Cl^- bound closely to the substrate in the active site of the *Vibrio alginolyticus* AP. For VAP, the charged residue in closest proximity to the SO_4^{2-} ion in the active site, to which the Cl^- might be binding, are Arg129, His277, and His465 (Figure 9). Cl^- could also be coordinated to the Zn ions, and be outcompeted by OH^- ions as pH increases as discussed above.

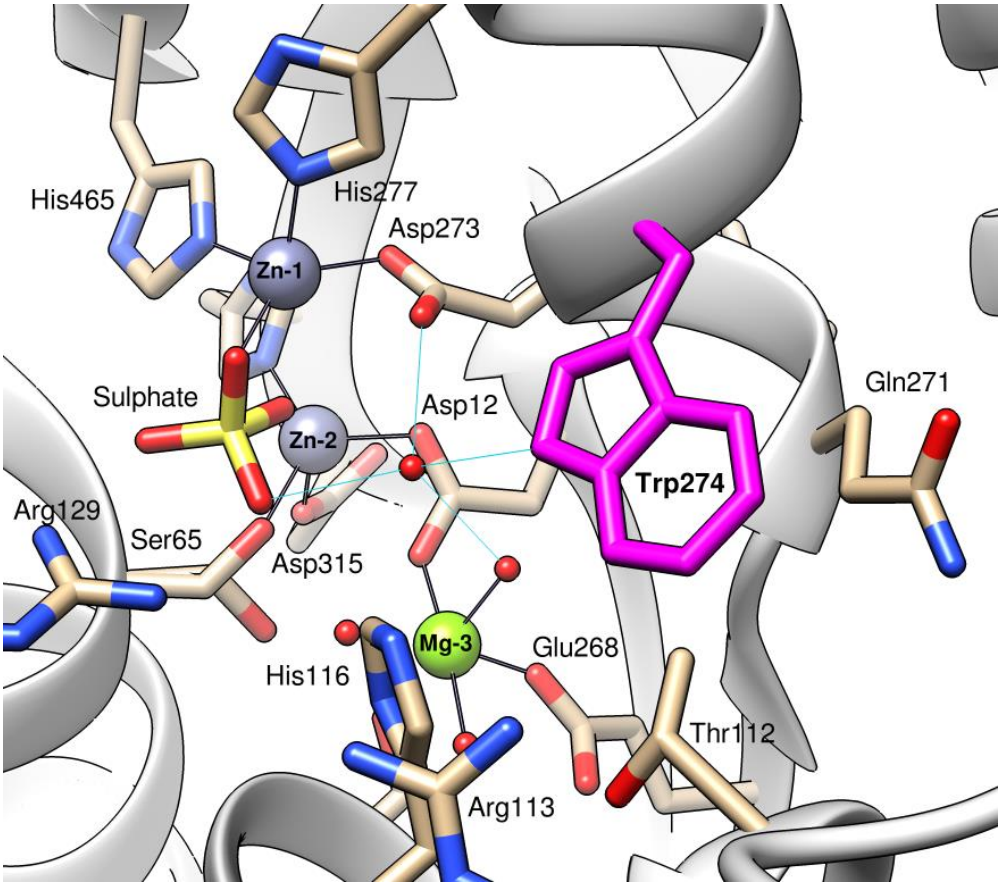

Figure 9. The active site structure of VAP showing residues in proximity to metal ligands and Trp274 (PDB: 3E2D). Trp274 is shown in magenta and the two Zn^{2+} ions in navy-purple. The Mg^{2+} ion is depicted in bright green connected with black lines with its ligands, including two water molecules. Water molecules are represented as red spheres and hydrogen bonds with aquamarine colored lines. A sulfate ion, binding as a competitive inhibitor, is shown in the active site. Note that the Ser65 is shown as two crystallographic rotamers [49].

VAP inactivation. Wild-type VAP was inactivated quite rapidly under low salt conditions at room temperature, well below the melting temperature of approximately 50°C (T_m). Our results indicated that this was not caused by dissociation of dimers to inactive monomers or dissociation of metal ions from the active site. We have previously reported that VAP can be transformed to an inactive dimer by concentrations of urea not sufficiently high to cause full denaturation [12]. The present work adds the information that this form of VAP is fully metalated (Figure 5). A deprotonation event was apparently important for maintaining the stability of the active site since $T_{50\%}$ increased from 25.8°C to 33.2°C by increasing the pH from 8.0 to 10.5 in a buffer of low ionic strength. The inactivated form was not easily converted back to the active enzyme, as various of our experiments with that aim have failed. It may be suggested that some key residue becomes locked in an unfavorable rotameric position by association with a partner of an opposite charge, but further studies on VAP variants are needed to substantiate this idea.

Direct measurements of dimer-monomer equilibrium are rare for APs. It is not trivial to obtain a signal for the dissociation of the identical monomers using biophysical methods. Sedimentation velocity experiments have been widely used [50-53], as have size exclusion chromatography (SEC) [12, 53, 54] and polyacrylamide electrophoresis [55, 56]. Some of these methods involve interaction of the protein with a matrix that may perturb the equilibrium.

Here, we measured the dimer dissociation constant for VAP by measuring specific activity after dilution. The dissociation constant was greatly affected by pH. The K_d was close to 1 nM

at pH 10.5 compared to 10–50 nM observed at pH 8.0 under the conditions tested. Inorganic phosphate in the medium (1.0 mM) was shown to increase the K_d of the dimer at pH 8.0, but not at pH 10.5. This was expected, since at pH 10.5 the affinity of the enzyme for phosphate is low. Sodium chloride at 0.5 M increased both the K_d at pH 8.0 and pH 10.5 with a sigmoidal character at pH 8.0 that was not seen at pH 10.5. This indicated that, at pH 8.0, Cl^- was able to bind to a specific site but not at pH 10.5. The free energy reported here is in the range 45–55 kJ/mol, and is within the limits of 20–70 kJ/mol reported for the dissociation of other homodimers [57]. Denaturing VAP with urea and monitor the denaturation by Trp fluorescence gave a free energy change for monomer unfolding of 14 kJ/mol [12]. Thus, it is clear that dimer formation contributes greatly towards VAP structural stability. Our laboratory has previously assessed the dimer dissociation for Atlantic cod AP induced by guanidium chloride (GdmCl) [32] or urea [58] using SEC, Trp fluorescence, and activity. The free energy was 34 kJ/mol and 36 kJ/mol for dimer dissociation with GdmCl and urea, respectively.

The effect of pH on VAP Trp fluorescence. Since changes in VAP Trp fluorescence at different pH were in most cases accompanied by changes in activity, it is likely that W274, which is located in the active site, is the residue most openly affected by pH. However, we have previously shown, using a Trp to Phe substitution, that W274 does not contribute highly to the total Trp emission spectrum of VAP [12]. Interestingly, the emission was increased for the W274F variant compared to wild-type which suggested that W274 is likely a resonance energy transfer (RET) acceptor for other Trp residues. Thus, when W274 was no longer present, more energy was emitted as photons from the remaining Trp residues. There are a few residues close to W274 which could also act as intrinsic quenchers [59], explaining sensitivity to subtle structural changes, mainly Q271, H116, D273 and E268 (Figure 9). It is likely that D273 could act as a good quencher by excited state electron transfer since it is made electron poor by coordination

with the Zn^{2+}, and by a key water molecule, which is involved in coordinating the substrate, which also makes a hydrogen bond with the W274 residue.

The residues that might be deprotonated in the neutral pH range are either histidine or amine groups which are much more efficient quenchers in their charged states. It is, however, well known that amino acid residues can have extreme shifts in pK_a values when located in active sites or hydrophobic environments [60, 61], so further experimentation is needed for firmer conclusions.

Conclusion

We have shown that VAP is highly activated by anions and displays a two-peak pH activity profile due to a suggested conformational change in the pH range 9.0–10.5. This presumed conformational change leads to a loss of substrate and product affinity leading to a change in the rate-limiting step from the last step (release of the noncovalently bound product) towards dephosphorylation of the covalent intermediate. These changes correlated with changes in tryptophan fluorescence. The effect of NaCl on the activity is proposed to be two-fold in nature. First, the salt increased the rate of inorganic phosphate product release by directly binding to a charged group in the active site, most likely a Zn ion. This presumed binding of chloride to Zn would also greatly stabilize the enzyme towards thermal activation in the pH range 8.0–10.5. Second, NaCl was shown to affect the dimer dissociation constant with a sigmoidal character at pH 8.0, but not at pH 10.5, an indication of specific chloride ion binding at the group(s) involved in connecting the monomers, or shaping the monomers in a productive conformation for dimer formation. Finally, we have shown that the inactivation is not due to dimer dissociation or Zn/Mg ion dissociation, but more likely is due to a subtle conformational change in the active site, where key residues in catalysis might be kinetically trapped in an unfavorable position.

AUTHOR INFORMATION

Corresponding Author

* Corresponding authors: Jens Guðmundur Hjörleifsson, email: jgh4@hi.is and Bjarni Ásgeirsson, email: bjarni@hi.is.

Associated content

Supporting information. Detailed description of the overlap-PCR extension used for sub-cloning of VAP to pET11a vector. VAP production in Lemo21(DE3) cells. Effect of pH and additives in buffers on the molar extinction coefficient of para-nitrophenol. VAP steady-state enzyme kinetics at various pH. Schematic representation of enzyme preparation before Zn^{2+} and Mg^{2+} analyzes

Author Contributions

The manuscript was written through contributions of both authors. Both authors have given approval to the final version of the manuscript.

Funding Sources

Financial support from the Icelandic Research Fund (project 141619-051) and the Science Institute of the University of Iceland is gratefully acknowledged.

Acknowledgements. We want to thank Ottar Rolfsson and Arnar Sigurðsson at the Department of System Biology at the University of Iceland for providing us with access to the SpectraMax-M3 fluorescence plate reader and help with its operation.

Abbreviations.

VAP, *Vibrio sp.* alkaline phosphatase; ECAP, *E. coli* alkaline phosphatase; CIP, calf intestinal phosphatase; TNAP, tissue non-specific alkaline phosphatase; PLAP, human placenta alkaline phosphatase; pNPP, para-nitrophenyl phosphate; pNP, para-nitrophenol; DEA, diethanolamine; CD, circular dichroism; RET, resonance energy transfer; SEC, size-exclusion chromatography.

References

(1) Feller, G., and Gerday, C. (2003) Psychrophilic enzymes: hot topics in cold adaptation, *Nat Rev Microbiol 1*, 200-208.
(2) Pucci, F., and Rooman, M. (2017) Physical and molecular bases of protein thermal stability and cold adaptation, *Curr Opin Struct Biol 42*, 117-128.
(3) Talley, K., and Alexov, E. (2010) On the pH-optimum of activity and stability of proteins, *Proteins 78*, 2699-2706.
(4) Thomas, D. N., and Dieckmann, G. S. (2002) Antarctic sea ice: a habitat for extremophiles, *Science 295*, 641-644.
(5) Mock, T., and Thomas, D. N. (2005) Recent advances in sea-ice microbiology, *Environ Microbiol 7*, 605-619.
(6) Paterova, J., Rembert, K. B., Heyda, J., Kurra, Y., Okur, H. I., Liu, W. R., Hilty, C., Cremer, P. S., and Jungwirth, P. (2013) Reversal of the Hofmeister series: specific ion effects on peptides, *J Phys Chem B 117*, 8150-8158.
(7) Schwierz, N., Horinek, D., and Netz, R. R. (2015) Specific ion binding to carboxylic surface groups and the pH dependence of the Hofmeister series, *Langmuir 31*, 215-225.
(8) Stec, B., Holtz, K. M., and Kantrowitz, E. R. (2000) A revised mechanism for the alkaline phosphatase reaction involving three metal ions, *J Mol Biol 299*, 1303-1311.
(9) Stock, J. B., Rauch, B., and Roseman, S. (1977) Periplasmic space in *Salmonella typhimurium* and *Escherichia coli*, *J Biol Chem 252*, 7850-7861.
(10) Wilks, J. C., and Slonczewski, J. L. (2007) pH of the cytoplasm and periplasm of *Escherichia coli*: rapid measurement by green fluorescent protein fluorimetry, *J Bacteriol 189*, 5601-5607.
(11) Hauksson, J. B., Andresson, O. S., and Asgeirsson, B. (2000) Heat-labile bacterial alkaline phosphatase from a marine *Vibrio sp.*, *Enzyme Microb Technol 27*, 66-73.
(12) Hjorleifsson, J. G., and Asgeirsson, B. (2016) Cold-active alkaline phosphatase is irreversibly transformed into an inactive dimer by low urea concentrations, *BBA-Proteins Proteom 1864*, 755-765.
(13) Wilson, I. B., Dayan, J., and Cyr, K. (1964) Some properties of alkaline phosphatase from *Escherichia coli* transphosphorylation, *J Biol Chem 239*, 4182-4185.
(14) Bloch, W., and Schlesinger, M. J. (1974) Kinetics of substrate hydrolysis by molecular variants of *Escherichia coli* alkaline phosphatase, *J Biol Chem 249*, 1760-1768.
(15) Fernley, H. N., and Walker, P. C. (1968) Effect of sodium chloride on *Escherichia coli* alkaline phosphatase, *Biochem J 110*, 11-12.

(16) Hayashi, M., Unemoto, T., and Hayashi, M. (1973) pH- and anion-dependent salt modifications of alkaline phosphatase from a slightly halophilic *Vibrio alginolyticus*, *Biochim Biophys Acta 315*, 83-93.
(17) Harkness, D. R. (1968) Studies on human placental alkaline phosphatase. II. Kinetic properties and studies on the apoenzyme, *Arch Biochem Biophys 126*, 513-523.
(18) Hoylaerts, M. F., Ding, L., Narisawa, S., Van Kerckhoven, S., and Millan, J. L. (2006) Mammalian alkaline phosphatase catalysis requires active site structure stabilization via the N-terminal amino acid microenvironment, *Biochemistry 45*, 9756-9766.
(19) Fernley, H. N., and Walker, P. G. (1965) Kinetic behaviour of calf-intestinal alkaline phosphatase with 4-methylumbelliferyl phosphate, *Biochem J 97*, 95-103.
(20) Halford, S. E. (1971) *Escherichia coli* alkaline phosphatase. An analysis of transient kinetics, *Biochem J 125*, 319-327.
(21) Sun, L., Kantrowitz, E. R., and Galley, W. C. (1997) Room temperature phosphorescence study of phosphate binding in *Escherichia coli* alkaline phosphatase, *Eur J Biochem 245*, 32-39.
(22) Orhanovic, S., and Pavela-Vrancic, M. (2003) Dimer asymmetry and the catalytic cycle of alkaline phosphatase from *Escherichia coli*, *Eur J Biochem 270*, 4356-4364.
(23) Bryksin, A., and Matsumura, I. (2013) Overlap extension PCR cloning, *Methods Mol Biol 1073*, 31-42.
(24) Bryksin, A. V., and Matsumura, I. (2010) Overlap extension PCR cloning: a simple and reliable way to create recombinant plasmids, *Biotechniques 48*, 463-465.
(25) Pace, C. N., Vajdos, F., Fee, L., Grimsley, G., and Gray, T. (1995) How to measure and predict the molar absorption coefficient of a protein, *Protein Sci 4*, 2411-2423.
(26) Hofmeister, F. (1888) Concerning regularities in the protein-precipitating effects of salts and the relationship of these effects to the physiological behaviour of salts, *Exp. Pathol. Pharmakol. 24*, 247-260.
(27) Hofmeister, F. (1888) On the water withdrawing effect of salts, *Arch. Exp. Pathol. Pharmakol 25*, 1-30.
(28) Sengupta, R., Pantel, A., Cheng, X., Shkel, I., Peran, I., Stenzoski, N., Raleigh, D. P., and Record, M. T., Jr. (2016) Positioning the intracellular salt potassium glutamate in the Hofmeister series by chemical unfolding studies of NTL9, *Biochemistry 55*, 2251-2259.
(29) Greaney, G. S., and Somero, G. N. (1979) Effects of anions on the activation thermodynamics and fluorescence emission spectrum of alkaline phosphatase: evidence for enzyme hydration changes during catalysis, *Biochemistry 18*, 5322-5332.
(30) Poe, R. W., Sangadala, V. S., and Brewer, J. M. (1993) Effects of various salts on the steady-state enzymatic activity of *E. coli* alkaline phosphatase, *J Inorg Biochem 50*, 173-180.
(31) Garen, A., and Levinthal, C. (1960) A fine-structure genetic and chemical study of the enzyme alkaline phosphatase of E. coli. I. Purification and characterization of alkaline phosphatase, *Biochim Biophys Acta 38*, 470-483.
(32) Asgeirsson, B., Hauksson, J. B., and Gunnarsson, G. H. (2000) Dissociation and unfolding of cold-active alkaline phosphatase from atlantic cod in the presence of guanidinium chloride, *Eur J Biochem 267*, 6403-6412.
(33) Gudjonsdottir, K., and Asgeirsson, B. (2008) Effects of replacing active site residues in a cold-active alkaline phosphatase with those found in its mesophilic counterpart from *Escherichia coli*, *FEBS J 275*, 117-127.
(34) Beauchamp, D. L., and Khajehpour, M. (2012) Studying salt effects on protein stability using ribonuclease t1 as a model system, *Biophys Chem 161*, 29-38.
(35) Zhao, H. (2005) Effect of ions and other compatible solutes on enzyme activity, and its implication for biocatalysis using ionic liquids, *J Mol Catal B-Enzym 37*, 16-25.

(36) Von Hippel, P. H., and Schleich, T. (1969) Ion effects on the solution structure of biological macromolecules, *Acc Chem Res 2*, 257-265.
(37) Baldwin, R. L. (1996) How Hofmeister ion interactions affect protein stability, *Biophys J 71*, 2056-2063.
(38) Zhang, Y. J., and Cremer, P. S. (2009) The inverse and direct Hofmeister series for lysozyme, *P Natl Acad Sci USA 106*, 15249-15253.
(39) Yang, Z., Liu, X. J., Chen, C., and Halling, P. J. (2010) Hofmeister effects on activity and stability of alkaline phosphatase, *Biochim Biophys Acta 1804*, 821-828.
(40) Norne, J. E., Szajn, H., Csopak, H., Reimarsson, P., and Lindman, B. (1979) The relation between activity and zinc and chloride binding of *Escherichia coli* alkaline phosphatase, *Arch Biochem Biophys 196*, 552-556.
(41) Gettins, P., and Coleman, J. E. (1984) Chloride binding to alkaline phosphatase. ^{113}Cd and ^{35}Cl NMR, *J Biol Chem 259*, 11036-11040.
(42) O'Brien, P. J., and Herschlag, D. (2002) Alkaline phosphatase revisited: hydrolysis of alkyl phosphates, *Biochemistry 41*, 3207-3225.
(43) Lazdunski, C., and Lazdunski, M. (1969) Zn^{2+} and Co^{2+}-Alkaline Phosphatases of *E. coli*, *Eur J Biochem 7*, 294-300.
(44) Krishnaswamy, M., and Kenkare, U. W. (1970) The effect of pH, temperature, and organic solvents on the kinetic parameters of *Escherichia coli* alkaline phosphatase, *J Biol Chem 245*, 3956-3963.
(45) Chaidaroglou, A., and Kantrowitz, E. R. (1989) Alteration of aspartate 101 in the active site of *Escherichia coli* alkaline phosphatase enhances the catalytic activity, *Protein Eng 3*, 127-132.
(46) Hinberg, I., and Laidler, K. J. (1972) The kinetics of reactions catalyzed by alkaline phosphatase: the effects of added nucleophiles, *Can J Biochem 50*, 1360-1368.
(47) Kim, T. H., Mehrabi, P., Ren, Z., Sljoka, A., Ing, C., Bezginov, A., Ye, L., Pomes, R., Prosser, R. S., and Pai, E. F. (2017) The role of dimer asymmetry and protomer dynamics in enzyme catalysis, *Science 355*.
(48) Papaleo, E., Renzetti, G., Invernizzi, G., and Asgeirsson, B. (2013) Dynamics fingerprint and inherent asymmetric flexibility of a cold-adapted homodimeric enzyme. A case study of the *Vibrio* alkaline phosphatase, *Biochim Biophys Acta 1830*, 2970-2980.
(49) Helland, R., Larsen, R. L., and Asgeirsson, B. (2009) The 1.4 A crystal structure of the large and cold-active *Vibrio sp.* alkaline phosphatase, *Biochim Biophys Acta 1794*, 297-308.
(50) Schlesinger, M. J., and Barrett, K. (1965) The reversible dissociation of the alkaline phosphatase of *Escherichia coli*. I. Formation and reactivation of subunits, *J Biol Chem 240*, 4284-4292.
(51) Applebury, M. L., and Coleman, J. E. (1969) *Escherichia coli* alkaline phosphatase. Metal binding, protein conformation, and quaternary structure, *J Biol Chem 244*, 308-318.
(52) Snyder, S. L., Wilson, I., and Bauer, W. (1972) The subunit composition of *Escherichia coli* alkaline phosphatase in I M tris, *Biochim Biophys Acta 258*, 178-187.
(53) Fosset, M., Chappelet-Tordo, D., and Lazdunski, M. (1974) Intestinal alkaline phosphatase. Physical properties and quaternary structure, *Biochemistry 13*, 1783-1788.
(54) Krull, I. S., Stuting, H. H., and Krzysko, S. C. (1988) Conformational studies of bovine alkaline phosphatase in hydrophobic interaction and size-exclusion chromatography with linear diode array and low-angle laser light scattering detection, *J Chromatogr 442*, 29-52.
(55) Al-Shawafi, H. A., Komaru, K., and Oda, K. (2017) Molecular defect of tissue-nonspecific alkaline phosphatase bearing a substitution at position 426 associated with hypophosphatasia, *Mol Cell Biochem 427*, 169-176.

(56) Olsen, R. L., Overbo, K., and Myrnes, B. (1991) Alkaline-phosphatase from the hepatopancreas of shrimp (*Pandalus borealis*) - a dimeric enzyme with catalytically active subunits, *Comp Biochem Phys B 99*, 755-761.
(57) Neet, K. E., and Timm, D. E. (1994) Conformational stability of dimeric proteins: quantitative studies by equilibrium denaturation, *Protein Sci 3*, 2167-2174.
(58) Asgeirsson, B., and Guojonsdottir, K. (2006) Reversible inactivation of alkaline phosphatase from Atlantic cod (*Gadus morhua*) in urea, *Biochim Biophys Acta 1764*, 190-198.
(59) Chen, Y., and Barkley, M. D. (1998) Toward understanding tryptophan fluorescence in proteins, *Biochemistry 37*, 9976-9982.
(60) Bashford, D., and Karplus, M. (1990) pK_a's of ionizable groups in proteins: atomic detail from a continuum electrostatic model, *Biochemistry 29*, 10219-10225.
(61) Mehler, E. L., Fuxreiter, M., Simon, I., and Garcia-Moreno E, B. (2002) The role of hydrophobic microenvironments in modulating pK_a shifts in proteins, *Proteins: Struct, Funct, Bioinf 48*, 283-292.